Fundamentals and Applications of Reflection FTIR Spectroscopy for the Analysis of Plasma Processes at Materials Interfaces

Guido Grundmeier,* Achim von Keudell, Teresa de los Arcos

Plasma processes are widely used for the deposition of thin films and/or the functionalization of material surfaces and interfaces ranging from inorganic to organic structures. The characterization of such plasma-modified surfaces is challenging and most efficiently performed by optical methods, such as FTIR-spectroscopy and related techniques. The present review aims at bridging the gap between optical spectroscopy fundamentals and the application of such experimental techniques in plasma surface science and engineering. The first part of the review covers the most relevant theoretical aspects of different reflection FTIR-spectroscopy approaches; the second part presents the different applications of these principles for the investigation of surface processes induced by plasma. The applications take into account interaction of plasma with metal surfaces, semiconductors, and polymeric materials.

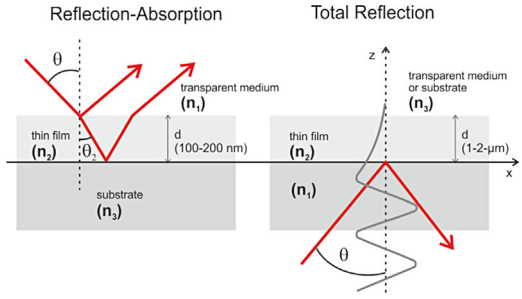

1. Introduction

Plasma processes are ubiquitous in the modern world and the cornerstone of many manufacturing technologies. Plasma-deposition or -etching techniques are regularly employed for the production of thin films or nanostructured materials for applications in the automotive, the microelectronics or medical industry, where superior materials performance and quality are needed (one prominent example is the fabrication of integrated circuits based on plasma etching of thin trenches with high-aspect ratios, which can only be realized by a clever use of reactive plasma processes). The common aspect in all these applications is that reactive plasmas are interfaced with a solid, so that the final quality of the deposited film, or the accuracy of an etched nanostructure, depends on the precise nature of the surface reactions. Consequently, the investigation of plasma surface processes and how these processes influence the quality of plasma-deposited films, are at the core of disciplines such as surface science, chemical engineering, plasma physics, and plasma chemistry; the consequence being that many different theoretical and experimental approaches are being developed to address different aspects of these research questions. The field of surface diagnostics is very broad, and it has successfully employed probing beams of electrons, ions, and photons. As a result, surface processes such as hydrogen adsorption on metals have been elucidated by in situ experiments in great detail.

Typically, thin and ultra-thin films, or interfaces, are characterized ex situ by infrared analysis in combination with X-ray electron spectroscopy and ToF-SIMS. However, the in situ analysis of plasma surface interactions by

Prof. G. Grundmeier, Dr. T. de los Arcos
Chemical Engineering and Macromolecular Chemistry, University of Paderborn, Warburgerstraße 100, 33098 Paderborn, Germany
E-mail: guido.grundmeier@uni-paderborn.de
Prof. A. von Keudell
Application Oriented Plasmas, Ruhr University Bochum, Universitätsstraße 150, 44780 Bochum, Germany

DOI: 10.1002/ppap.201500087

traditional and well established surface diagnostics is challenging. On the one hand, plasma-exposed surfaces are usually not well defined single crystal facets; on the other hand, the incident species in a plasma process consist of a usually non-characterized mixture of ions, radicals, electrons, and photons. Furthermore, analyzing the surface interaction of those plasma-present species separately might not capture the complete plasma surface interaction due to emergence of synergisms or anti-synergisms among the different species. There exist few cases of particle beam experiments dedicated to the study of plasma relevant heterogeneous surface reactions, but their applicability is limited to selected examples, such as the interaction of fluorine beams with silicon or the interaction of hydrogen and methyl radicals with carbon surfaces.

The challenge of an in situ analysis of plasma surface interactions can be overcome by using real-time diagnostics. The use of traditional surface diagnostics in real-time during plasma processing, however, remains difficult due to the typical pressure range of plasmas, which spreads typically from some tenths of Pa, to atmospheric pressure. Most surface diagnostics such as low energy electron diffraction (LEED), PE, IPE, etc., are based on the interaction of low-energy electron beams with the surface of interest, which require ultra-high vacuum conditions incompatible with a real time measurement of a plasma-exposed surface.

By comparison, optical diagnostics are perfectly suited to address that challenge because they can be applied both ex situ and in situ, and by a clever design of the optical setups, they can also be made surface sensitive. In particular, infrared spectroscopy is most powerful, because it probes the vibrational response of the molecules at the surface or in the plasma-deposited film and allows to monitor changes in composition and functionality of the thin films.

The aim of this review is thus to present both the fundamentals and selected experimental approaches of in situ reflection Fourier Transform Infrared Spectroscopy (FTIR) spectroscopy methods with a focus on the application in plasma interface chemistry. Reflection FTIR spectroscopy is most widely used to characterize polymer interface processes as specific selection rules, or, under certain conditions, a specific surface enhancement allows for an enhanced sensitivity for ultra-thin film analysis or an interface sensitive analysis. In this review, we have divided FTIR-reflection spectroscopy methods into external and internal reflection modes (Figure 1), which will be briefly discussed. The possibility of FTIR surface enhancement, based on the increase of the field strength induced by surface plasmon resonance in the case of metallic substrates or by constructive interference in a resonant structure in the case of insulator surfaces will be also discussed. We will furthermore briefly describe Sum Frequency Generation (SFG), as a related nonlinear spectroscopy with molecular interface sensitivity and very specific selection rules.

2. Fundamentals of FTIR-Reflection Spectroscopy

2.1. External Reflection on Metals: Infrared Reflection-Absorption Spectroscopy (IRRAS)

External reflection spectroscopy is most surface sensitive on highly reflecting metals. The macroscopic response of a solid to electromagnetic radiation is the basis for a quantitative description of infrared reflection absorption spectroscopy. Excellent reviews on the fundamentals of the relevant optics can be found in ref. [1,2] In this presented review, the aim is to qualitatively describe the methods and to hint at the experimental aspects most relevant to the investigation of plasma-related surface modifications.

At an interface, the electromagnetic fields are calculated by solving Maxwell's equations. In combination with the respective boundary conditions for the studied system, it is possible to evaluate the components of the electric field at the position of the adsorbed film. In case of metal substrates, their large dielectric function leads to a normal component of the electric field on the gas phase side of the interface which is much larger than that on the substrate side. In the case of the tangential components (the components of the electric field perpendicular to the plane of incidence), the amplitudes before and after reflection are close in magnitude but opposite in sign (the phase shift at the reflecting surface is 180°), thereby forming a node at the surface. The normal component of the light which is polarized parallel to the plane of incidence does not suffer such a phase shift so that the reflected field adds constructively to the incident field.

From the above described processes, a so-called selection rule follows, which is simply illustrated by looking at the superimposition of dipoles and image dipole at the interface (Figure 1b). A vibrating dipole of surface species is accompanied by an image dipole within the metal.[1] Although a dipole vibrating normal to the surface leads to an image dipole parallel to the dipole of the surface adsorbates, a dipole parallel to the metal surface leads to an image dipole oriented antiparallel, resulting in the compensation of the infrared active transition dipole moment.

The amplitude of the electric field oscillating normal to the metal surface is strongly dependent on the angle of incidence and shows a maximum at grazing incidence.[3] However, in many cases, experimental concerns lead to a compromise between surface enhancement and infrared intensity that can be guided through the reflection cell.

McIntyre and Aspnes derived a linear approximation theory[4] that allows for a quantitative treatment of the reflection spectra. It is assumed that collimated IR-light of

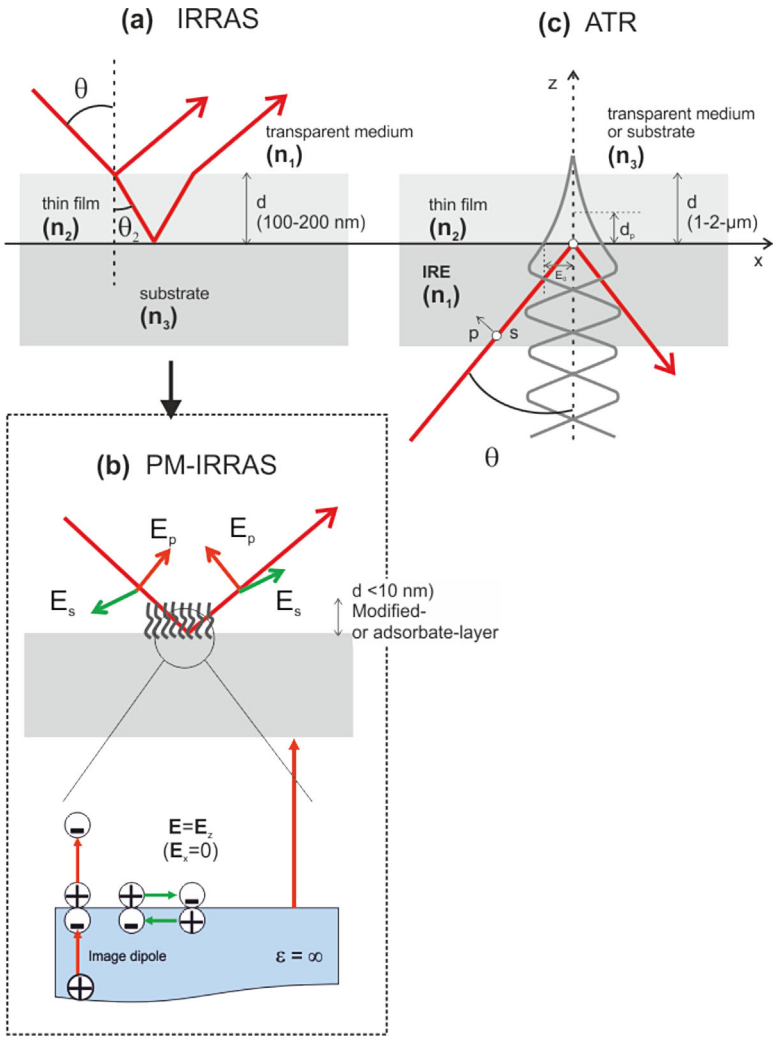

Figure 1. Schematic representation of different reflection techniques used for infrared spectroscopy. (a) Infrared reflection absorption spectroscopy (IRRAS), particularly useful for the case of metallic substrates. (b) Polarization-modulated IRRAS (PM-IRRAS): while the s-component of the electric field gets reversed at the surface during reflection and gets canceled, the p-component adds to a non-zero vector. Therefore, only p-polarized light can carry surface information. (c) Attenuate internal reflection (ATR), useful for the observation of surface species on solid transparent materials with high-refractive index.

wavelength λ enters from the gas phase at an angle θ on a homogeneous isotropic thin film of thickness d, which covers a highly reflecting homogeneous and isotropic metal substrate (see the three-layer model in Figure 1a). As discussed before, the parallel and the perpendicular polarization of light with regard to the plane of incidence are considered separately. Based on the corresponding Fresnel equations it is possible to derive a linear formulation for the normalized reflectance change due to the presence of the thin film, with the bare substrate acting as reference. For the simplified equation, will be assumed that the dielectric constant of the metal substrate is much higher than that of the absorbed film.

For the parallel component, the change of reflectance depends on the optical properties of the film and on the angle of incidence. If $n_2 \gg k_2$, which is in many cases valid, we obtain[1]

$$\left(\frac{R_d - R_0}{R_0}\right) = \left(\frac{\Delta R}{R_0}\right) = -\frac{4\sin^2\theta}{n_2^3\cos\theta}\alpha \cdot d = -f \cdot \alpha \cdot d \quad (1)$$

where α is the absorption coefficient of the film, and f is the defined as a sensitivity factor $f = 4\sin^2\theta/n_2^3\cos\theta$ that compares the measurement at normal incidence with that at grazing incidence. The quantity $4\sin^2\theta/n_2^3$ represents the enhancement of the electric field vector, whereas the remaining factor $(\cos\theta)^{-1}$ corresponds to the area of film probed by a light beam of unit cross section area.

For small film thickness values ($d \ll \lambda$), the measured absorbance is approximately proportional to the film thickness. It can be shown that the value d/λ_0 (where λ_0 is the shortest wavelength in the measured spectrum) should be smaller than 0.01 for high-sensitivity measurements and an almost linear dependence of film thickness and reflectance change. This means that the film thickness should be ideally below 100 nm.

However, the peak positions in infrared spectroscopy cannot be directly compared to transmission FTIR-data without caution. Especially, for molecular groups with high-extinction coefficients such as carboxyl groups, peak shifts in comparison to transmission data are observed.[2,5]

2.2. Polarization-Modulated Infrared Reflection-Absorption Spectroscopy (PM-IRRAS)

A very useful development of IRRAS, which is of particular interest for the investigation of adsorbates, is polarization modulation spectroscopy. This technique exploits the selection rules of IR light incident under grazing incidence on a metal substrate.[2,6] The phase change upon reflection

Plasma Process. Polym. **2015,** *12*, 926–940

DOI: 10.1002/ppap.201500087

for perpendicular polarization is 180°, independent of the angle of incidence, whereas for parallel light it is sensitive to the variation of the angle of incidence. The result is that the intensity of the electric field at the metal surface for parallel polarized light rises with increasing angle of incidence, reaching a maximum near the grazing incidence. In contrast, the intensity of the electric field for perpendicular-polarized light is negligible for all angles of incidence. Therefore, only the light that is polarized parallel to the plane of incidence carries information about the adsorbed species on the surface. Due to the random orientation of gas phase molecules, their absorption is independent of the orientation of the electric field vector. Phase modulated spectroscopy thus eliminates the absorption from the sample environment.

The polarization can be simply done by recording two IR spectra in parallel and perpendicular polarizations, respectively, in which case, we will talk of discrete polarization modulation (referred to, in the following, as FT-IRRAS).[7] In this case, the measurements provide two absorption spectra according to

$$A_p = -log\left(\frac{I_p}{I_{0p}}\right) \quad A_s = -log\left(\frac{I_s}{I_{0s}}\right) \tag{2}$$

where A_p is the absorption for parallel-polarized light and A_s is the absorption for perpendicular-polarized light. The parallel absorption consists of both the gas phase absorption and the film absorption, while for the perpendicular absorption the latter is missing. Moreover, the gas phase absorption is identical for both components because of the random orientation of molecules in the gas phase. Hence, the difference $A = A_p - A_s$ is due only to the absorption of the surface layer.

In so-called polarization modulation infrared reflection-absorption spectroscopy (PM-IRRAS) p- and s-polarized light are measured simultaneously under grazing incidence and modulated at high frequencies, thus allowing to obtain a differential reflectance spectrum of the surface and adsorbed layers. Apart from the removal of gas phase absorption, another gain is that no reference measurement is necessary, which is of advantage for the analysis of surface states that do not allow for the preparation of clean references. A schematic of a typical setup is shown in Figure 2.

In PM-IRRAS, IR light from the Michelson interferometer of a FTIR spectrometer is directed through a polarizer toward a photoelastic modulator (PEM).[6] The PEM modulates the infrared beam by rotating the polarization of the light sinusoidally at the frequency of the birefringence modulation introduced mechanically in a zinc-selenite (ZnSe) crystal. After the monochromatic incident, infrared beam (linearly polarized 45° to the strain axis) passes through the modulator, the intensity is given by

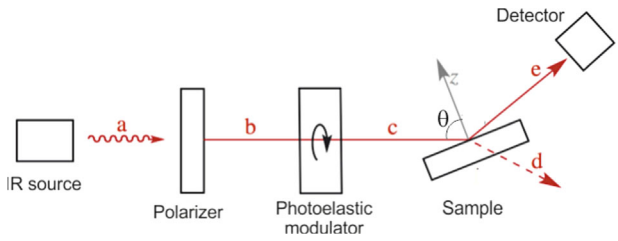

Figure 2. Typical schematic setup for PM-IRRAS. (a) Raw IR beam; (b) polarized IR beam; (c) phase modulated IR beam; (d) diffracted beam; (e) reflected IR beam; θ, incidence angle. Figure modified from ref.[56]

$$I(t) = \frac{\left[I_p + I_s + \left(I_p - I_s\right) \cdot \cos(\Phi_0 \cos(\chi t))\right]}{2} \tag{3}$$

where I_p and I_s being the intensities of p- and s-polarized light, respectively, χ the modulation frequency of the PEM, and Φ_0 a constant that depends linearly on the amplitude of mechanical modulation of the PEM. This modulation appears as a high-frequency signal on the interferogram. The two modulation frequencies from interferometer (low) and PEM (high), are then separated by dedicated electronics. The low-frequency signal is the average interferogram (I_A); the high-frequency signal (typically 100 kHz modulation signal) represents the difference interferogram (I_D), which is demodulated by an external lock-in amplifier and sent back to the electronics. After the Fourier transformation the average and the difference spectra are calculated to be[8]

$$I_A(\varpi) = \frac{(I_p + I_s)}{2} \quad I_D(\varpi) = \frac{(I_p - I_s)}{2} \tag{4}$$

where ϖ is the wavenumber. The differential reflectance spectrum is defined as

$$\frac{\Delta R}{R} = \frac{I_D(\varpi)}{I_A(\varpi)} \cdot J_2(\Phi_0), \tag{5}$$

where $J_2(\Phi_0)$ is the second-order Bessel function, which multiplies the differential spectrum due to the different reflectivity of I_P and I_S radiation at a metal interface.

The amplitude of the mechanical excitation of the PEM crystal defines the points of the zero crossings of the Bessel function. The appropriate setting for the amplitude depends on the experiment, i.e., on the wavelength region of interest. The intensity increases linearly with the film thickness for small film thickness values.

2.3. Internal Reflection: Attenuated Total Reflection (ATR) Spectroscopy

The observation of surface species on solid transparent materials with high-refractive index, such as most

semiconductors is best achieved using internal reflection methods. Attenuated total reflection spectroscopy (ATR) is based on the phenomenon of total internal reflection and the generation of an evanescent field at an internal reflection element (IRE)/sample interface (Figure 1c).[3] Excellent reviews are provided by ref.[1,2]

According to Chabal,[2] if the substrate is non-absorbing but still characterized by a high index (the permittivity ε is real and $\varepsilon \gg 1$), as is the case for a number of semiconductors, it is possible to consider radiation internally incident on the interface. For angles of incidence greater than the critical angle, the radiation is totally internally reflected. According to Snell's law $n_1 \sin\theta = n_2 \sin\theta_2$, the critical angle θ_{crit} for which total internal reflection occurs is provided by the following relation: $\sin\theta_{crit} > \sin\theta = n_2/n_1$. In this case, the superimposition of the electric field of the incident and the reflected light leads to an evanescent field decaying exponentially into the rarer medium (Figure 1c).

For an absorbing medium with dimensions significantly larger than the evanescent field penetration depth, the probed depth d_p depends on the wavelength of the incident radiation, the angle of incidence and the refractive index of the IRE (n_1) and the medium (n_2). However, the spectral information obtained is the average over the wave, which decays exponentially with the distance from the surface. The evanescent field penetration depth is usually in the micrometer range and is calculated according to the following equation, as the depth for which the amplitude of the evanescent field drops to $^1/_e$ of the value at the interface.[3]

$$d_p = \frac{\lambda}{2\pi n_1 \sqrt{\left(\sin^2\theta - \left(\frac{n_2}{n_1}\right)^2\right)}} \tag{6}$$

where n_1 is the refractive index of the optically denser medium, n_2 is the refractive index of the propagating (rarer) medium, θ is the angle of incidence, and λ is the wavelength. The equation shows that the penetration depths decreases and thereby the interphase sensitivity increases with the refractive index of the IRE and an increasing angle of incidence. With an increasing wavelength of light the penetration depth increases linearly.

ATR spectroscopy provides information from the interphase region within depths between a few hundred nanometers up to few micrometers, where the information depth is dependent on the angle of incidence and the refractive index of the ATR crystal. A thickness dependence of the measured absorbance can be calculated when the film thickness is significantly smaller than the penetration depth of the evanescent light. This is a typical situation for the FTIR-ATR study of plasma/materials interactions. In such a measurement, the evanescent field has a significant intensity even in the medium (n_3) above the thin film (Figures 1 and 3). For thin films, we assume that the intensity of the field is almost constant over the film thickness.

If we wish to compare the sample absorbance of the ATR measurement with that of a transmission measurement, we need to calculate the volume of the evanescent wave, known as the effective penetration of the IR beam. The effective penetration d_p (see Figure 3) is different for parallel polarization (d_{ep}) and perpendicular polarization (d_{es}) and their values can be approximated by the following equation[3]:

$$\begin{aligned} d_{ep} &= \frac{4n_{21}\cos\theta\left[(1+n_{32}^4)\sin^2\theta - n_{31}^2\right]}{(1-n_{31}^2)\left[(1+n_{31}^2)\sin^2\theta - n_{31}^2\right]} \cdot d \\ d_{es} &= \frac{4n_{21}\cos\theta}{(1-n_{31}^2)} \cdot d \end{aligned} \tag{7}$$

where $n_{ij} \equiv n_i/n_j$ represent the ratio between the respective refraction indices and d is the thin film thickness. It turns out that the intensities of the absorption bands of the film increase with film thickness d and are independent of the wavelength of light. Moreover, the equations imply that the critical angle is related to n_{31} instead of n_{21} in volume spectra. This means that for thin film spectroscopy by ATR the anomalous dispersion is not as critical as for volume spectra.

2.4. Optical Cavity Substrates

To improve the sensitivity of non-enhanced ATR measurements, multiple internal reflections can be applied using

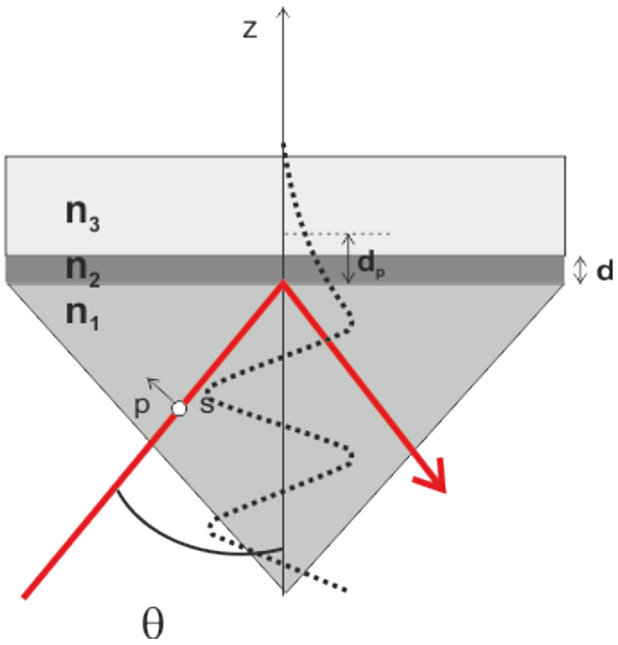

Figure 3. Schematic for reflection measurements on a thin film using internal reflection spectroscopy (ATR).

Plasma Process. Polym. **2015,** *12*, 926–940

DOI: 10.1002/ppap.201500087

specially designed optical crystals, such as the so-called optical cavity substrates (OCS).[9–11] The OCS is an optically resonant multilayer structure consisting of a double-polished c-Si (100) wafer with a dielectric spacer of SiO_2 on both sides and a metal reflector on the back side. The SiO_2 layers are formed simultaneously by wet oxidation of the Si for 4 h at 1100 °C, with a final short oxidation step in O_2 in order to reduce the H content in the oxide. The back side is coated with Al by means of thermal evaporation, and the film of interest is deposited on the top side (Figure 4).

The reflectance of a thin film on top of an OCS can be calculated using the Fresnel coefficients t and r at each boundary, the angle of incidence θ and the phase coefficients β_{film} of every layer in the system.[12] The latter are defined as

$$\beta = \frac{2\pi}{\lambda} nd\cos\theta, \tag{8}$$

where n and d are the refractive index (real part) and thickness of the layer in the system, respectively, and θ the angle under which the light is propagating in that layer with respect to the surface normal.

The wavelength resolution determines the corresponding coherence length, which should be compared with the layer thicknesses in the system. IR studies typically involve one or more thin films with a thickness of nanometer to micrometer, deposited onto a Si substrate with a thickness of several 100 μm. At wavelength resolutions $>4\,cm^{-1}$, the coherence length is larger than the thickness of the film(s) but smaller than the substrate thickness. Therefore, the light propagation is coherent in the thin film(s) and incoherent in the substrate. An exact optical model to simulate the IR reflectance is based on the coherent transmission and reflection of the top (thin film/oxide) and of the backside (oxide/metal) with R_{film} being the reflection at the film surface; T_{film} is the transmission of light incident from the ambient to the Si substrate through the film on oxide; R_{top} is the reflection of light incident from the substrate to the back of the film on oxide; R_{bottom} is the reflection of the light incident from the substrate to the backside layers; and T_{top} is the transmission from the substrate to the ambient through the film on oxide. The reflection of the whole system, with Im ($\beta_{substrate}$) as the imaginary part of the phase coefficient of the silicon substrate, is then[9,13–16]

$$R_{total} = R_{film} + \frac{T_{top}T_{film}R_{bottom}\exp(-4\mathrm{Im}(\beta_{substrate}))}{1 - R_{bottom}R_{top}\exp(-4\mathrm{Im}(\beta_{substrate}))} \tag{9}$$

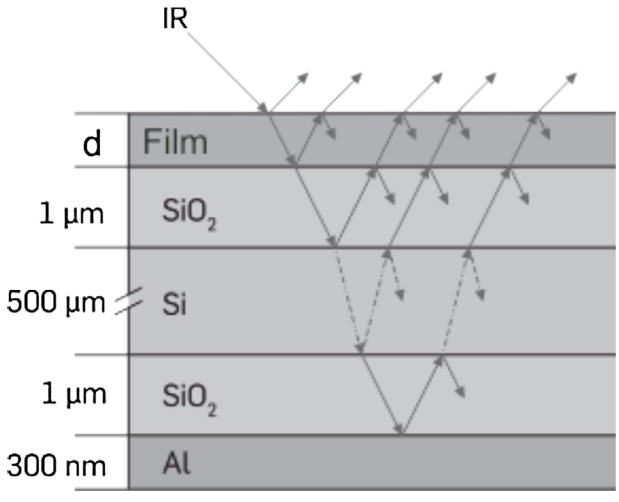

Figure 4. Schematics of an optical cavity substrate (OCS), adapted from Große-Kreul et al.[48]

The OCS has to be adapted to a specific measurement problem, because the signal enhancement is only achieved for specific wavenumber ranges. Thus, the above equation can be used to describe the reflectance of a thin film on a Si substrate by setting the thickness of the oxide layers to 2 nm (equivalent to native oxide layers) and omitting the metal backside coating (by setting the refractive index of the Al coating artificially to $n_{Al} = 1 - i0$. In a similar manner, this equation can be used to describe the reflectance of a thin film on a metal substrate by setting the thickness of the Si wafer and of the oxide layers to 0 nm. If the silicon-hydrogen stretching vibrations are monitored at a silicon surface, the enhancement has to be optimized for 2000 cm^{-1} yielding an optimal oxide thickness for the OCS of 1040 nm.

As an example, Equation (9) is used to calculate the change in reflectivity ΔR caused by the presence of a thin a-Si:H top layer ($d = 1$ nm, $n_{top\ layer} = n - i0.04$) on an OCS, using an s-polarized beam at an incidence angle of 70°. The wavenumber is set at 2000 cm^{-1} because the stretching modes of Si–H bonds are clustered around this position (1985–2140 cm^{-1}). Figure 5 compares this change in reflectivity in comparison to normal transmission, to reflection at a metal substrate and to the reflection at 80° at a bare silicon surface. One clearly sees that a superior signal enhancement is achieved over a wide refractive index range.

The real part n of the refractive index $n_{top\ layer}$ is varied in order to compare the sensitivity for surface modes (which experience a low-refractive index) versus bulk modes (which experience a high-refractive index). ΔR is large over the entire range of refractive indexes and one order of magnitude larger compared to ΔR of the very same layer on a bare silicon wafer. This signal enhancement occurs when the electric field strength is large at the location of the absorbing thin film. In the case of the optical cavity substrate, the electric field vectors of the light waves in s-polarization undergo constructive interferences at the

oxide interfaces for each external (T_{film}, R_{film}) or internal reflection (T_{top}, R_{top}, R_{bottom},) for a given wavenumber and oxide thickness. Because the multiple reflections inside the Si wafer are phase incoherent, the light intensities of the internal reflections (T_{top}, R_{top}, R_{bottom}) sum up, and no destructive interferences occur among them. Due to the working principle of the OCS, the maximum signal enhancement is only achieved for a single resonance frequency ω_0. This maximum, however, is rather broad and provides a reasonable signal enhancement also for $\omega_0 \pm 200\ cm^{-1}$.

The use of an OCS has several advantages: (i) it is equally sensitive to surface and bulk modes; (ii) all infrared light reaches the detector by using an Al backside coating; (iii) the probe area has the size of the focused IR spot on the sample; (iv) the OCS is easy to manufacture and align in the IR setup; (v) the signal enhancement depends on the film thickness. The resonant structure (see above) of the optical cavity can be tuned for good signal enhancement at an arbitrary film thickness. The main limitations of OCS, on the other hand, are as follows: (i) the initial surface consists of an amorphous SiO_2 film; (ii) the signal enhancement is wavenumber sensitive; (iii) IR spectra acquired with high-wavenumber resolution are harder to interpret due to the appearance of fringes caused by coherence in the Si wafer; (iv) the signal enhancement is sensitive to the film thickness; (v) the oxide needs to be transparent in the wavenumber range of interest; (vi) only s-polarization is used.

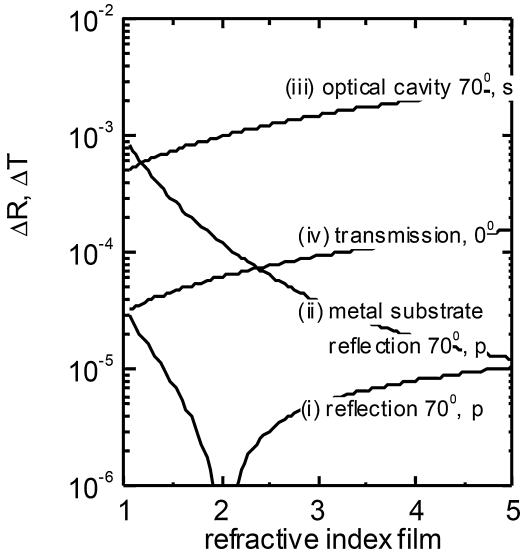

Figure 5. Change in reflectivity at 70° incidence angle due to the presence of a thin film ($n = n - i0.04$, thickness 1 nm) with varying refractive index n on top of three different substrates: (i) crystalline silicon in p polarization; (ii) metal substrate in p polarization; (iii) optical cavity substrate in s polarization; and (iv) change in transmission at normal incidence. From von Keudell and Abelson.[11]

2.5. Surface Enhanced FTIR-Spectroscopy

For both the internal and external reflection modes, surface enhanced FTIR spectroscopy has been proposed in order to achieve even higher sensitivity for ultra-thin films or molecular layers and to enhance the interface selectivity of the analysis. The most commonly applied substrates that enable surface-enhanced infrared absorption (SEIRA) are island films of the coinage metals Au, Ag, and Cu. However, SEIRA has also been demonstrated on a variety of other metals including Pt,[17] Sn,[18] and Fe,[19] amongst others. Upon irradiation with light, surface plasmons are excited in the metal islands which results in a broad plasmon absorption peak extending from the visible to the mid-infrared spectral regions.[20] In the case of rather dense island films, the induced dipoles of neighboring islands can couple with each other, which leads to an additional redshift of the absorption band. When molecules are adsorbed on the metal islands, an enhancement of their infrared absorption is observed for the first few monolayers. This enhancement results from an enhanced electromagnetic field in the close vicinity of the metal islands and scales linearly with the absorption of the metal film.[20] However, the estimated electromagnetic field enhancement in the mid-infrared region is only about tenfold, in contrast to measured infrared absorption enhancement factors of up to 10^3. In order to account for such strong enhancement, additional dipoles in the metal islands induced by the adsorbed molecules have to be considered. The resulting optical perturbation will be largest at the vibration frequencies of the molecule, so that the absorption spectrum of the metal island film should correspond mostly to that of the adsorbed molecule.[21]

Effective medium theories incorporate both of these contributing effects and have been used quite successfully to model SEIRA experiments.[22] An additional minor contribution to the total enhancement might stem from orientation effects of the adsorbed molecules.[21] SEIRA is, however, not limited to metallic substrates as has been demonstrated by Anderson[23] who reported enhanced infrared absorption from molecular films deposited onto dielectric, i.e., SiC and Al_2O_3, micro- and nanoparticles. In analogy to metallic substrates where an electromagnetic field enhancement occurs upon photon absorption around the plasmon resonance, enhanced optical fields can be generated at the surface of the dielectric particles when they are illuminated at their surface phonon resonance frequency. This effect resulted in an enhancement factor exceeding 100 for SiC particles.

In 2000, Jensen et al. employed nanosphere lithography to fabricate nanostructured SEIRA substrates.[24] The resulting films consisted of ordered triangular Ag islands and exhibited a strong surface plasmon resonance in the mid-infrared. By optimizing the shape, size, and

DOI: 10.1002/ppap.201500087

arrangement of the islands, as well as combination with appropriate substrates, the position of the plasmon resonance could be tailored to coincide with the infrared bands of the analyte molecule, enabling resonant excitation of molecular vibrations. More recently, this approach has been extended to fabricate more complex nanoantennas by different lithographic techniques which yield SEIRA enhancement factors in the range of 10^5–10^6.[25–28]

2.6. Sum Frequency Generation

Sum Frequency generation (SFG) spectroscopy is a second-order nonlinear optical technique that registers the vibrational spectra at surfaces and interfaces. It is uniquely monolayer surface-sensitive, and therefore an excellent method to provide surface structure and surface composition via the vibrational spectrum. Being a second-order nonlinear optical process, it is forbidden under the electric-dipole approximation in media with inversion symmetry and it only is activated at the material surface where the symmetry inversion is broken. SFG is generated by two laser photons at frequencies of ω_{VIS} and ω_{IR} (in the visible and infrared region, respectively) and observed as a single photon whose frequency is the sum of the original laser photons $\omega_{SF} = \omega_{VIS} + \omega_{IR}$ (Figure 6). The SFG intensity is proportional to the square of the second-order nonlinear susceptibility of the medium, which can be decomposed into a non-resonant and resonant term

$$\chi^{(2)}(\omega_{SF} = \omega_{VIS} + \omega_{IR}) = \chi^{(2)}_{NR} + \chi^{(2)}_{R} \tag{10}$$

The resonant term $\chi^{(2)}_R$ can be expressed as:

$$\chi^{(2)}_R = \frac{N\langle\beta\rangle}{\varepsilon_0} \tag{11}$$

where N is the density surface molecules, β in this case, is, the molecular hyperpolarizability averaged over all molecular orientation on the surface, and ε_0 is the vacuum permittivity. Within the electric dipole approximation, β can be expressed as

$$\beta_{q,lmn} = \frac{\alpha_{q,lmn} \cdot \mu_{q,n}}{2\hbar(\omega_q - \omega_{IR} - i\Gamma_q)} \tag{12}$$

where $\alpha_{q,lmn}$ is the Raman tensor element, $\mu_{q,n}$ is the IR transition dipole moment, ω_q is the resonant frequency, and Γ_q is the damping constant of the qth molecular vibrational mode. As given by the Equation (12), the SFG signal is generated when both IR and Raman vibrational modes are active. The SFG intensity is enhanced when ω_{IR} is in resonance with an SF-active molecular vibrational mode as well as when ω_{SF} or ω_{VIS} are also resonant with an existing surface electronic state. In addition, the SFG signal is polarization dependent, enabling the detection of the average molecular orientation at the surface.

3. Applications of Reflection FTIR-Spectroscopy in Interface Plasma Science

3.1. Plasma-Metal Interfaces

Polarization modulation techniques have demonstrated to be ideally suited for the investigation of surface modifications induced by plasma on metallic substrates. The corrosion resistance and the adhesion of organic coatings, laminates, and adhesives on oxide covered metals are of crucial importance for many technical applications. Of particular relevance in de-adhesion and corrosion phenomena, is the adsorption of water on the oxide covered metal surface, which is the initiating process and which can be steered by activation of the surface.

The plasma oxidation of engineering metal substrates by means of low-temperature plasmas was mainly studied by Raacke et al.[29] using a combination of in situ FT-IRRAS, quartz crystal microbalance (QCM), and Kelvin Probe (KP) measurements (Figure 7). For metal substrates, such as iron and zinc, which form n-semiconducting oxide films, the authors showed that the redox state of the passive film and the hydroxylation can be influenced by reducing and oxidizing plasmas. Figure 8 shows the in situ FT-IRRAS data of a zinc–magnesium alloy after exposure to reducing and oxidizing plasmas.[30] By the effect of the reducing Ar plasma, initially adsorbing carboxylates and aliphatic groups are desorbed, whereas the oxidizing plasma leads to the formation of additional zinc oxides. By means of parallel in situ work function measurements and ex situ XPS data the authors could show that not only the oxide composition is changed but the

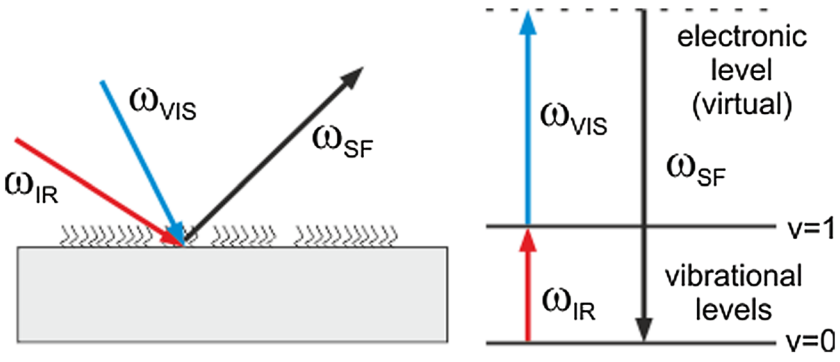

Figure 6. Schematic of experimental Sum Frequency Generation (SFG) setup for external reflection studies.

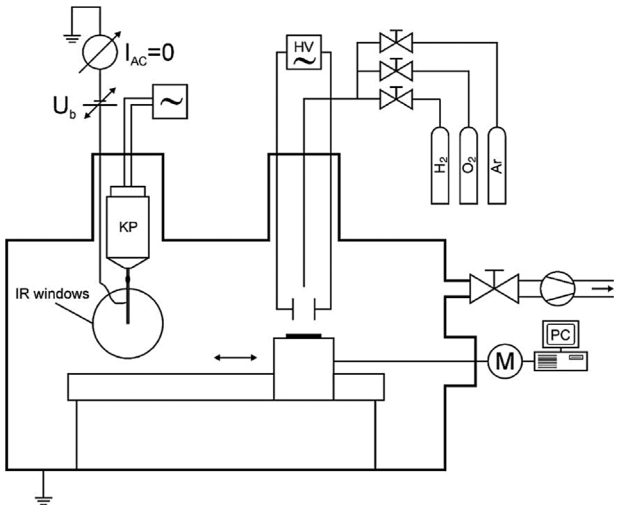

Figure 7. Experimental setup of a combination of in situ FT-IRRAS and Kelvin Probe (KP) with a plasma cell, ideally suited for the study of plasma modifications on metallic substrates. From Raacke et al.[29]

surface potential can be irreversibly changed to a desired value by the reductive or oxidative plasma treatment. The plasma surface treatment can thereby compete with wet-chemical electrochemical or high-temperature processes. It can be foreseen that the typical advantages of low temperature dry plasma processes will promote this application in the future.

For metals, such as aluminum, which form insulating oxide passive films, Giza et al.[31] showed that the hydroxylation degree of the surface can be achieved by varying the plasma gas composition from argon to oxygen and water. With increasing hydroxyl-forming gases in the plasma, the degree of hydroxylation increases (Figure 9). The authors could show that the increased hydroxylation advanced the kinetics of organic acid adsorption. Organophosphonic acid molecules adsorbed much faster on strongly hydroxylated surfaces than on surface which are rather oxide-like. The kinetics of adsorption were followed in situ by means of a QCM.

Giner et al.[32] also reported on the influence of plasmas surface treatment on the physisorption and chemisorption of water on oxyhydroxide film-covered aluminum surfaces by simultaneous QCM and PM-IRRAS studies. A plasma surface modification was employed to adjust the surface chemistry and film thickness prior to the study of the oxyhydroxide growth under atmospheric conditions. The low-pressure plasma treatments led to the effective removal of adsorbed organic contaminations. Additionally, the argon plasma treatment led to the reduction of the hydroxyl surface density and a reduction in the oxyhydroxide film thickness while the oxyhydroxide film thickness and the surface hydroxyl density were increased by the water plasma treatment.

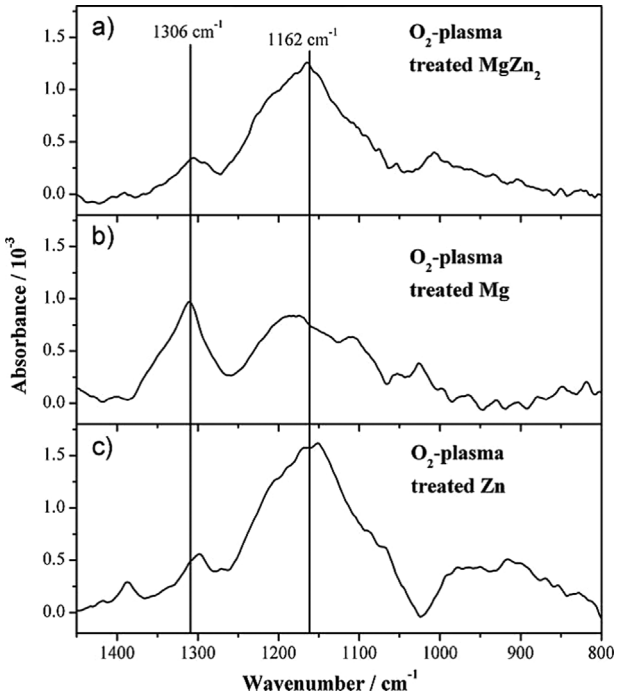

Figure 8. In situ FT-IRRA spectra on O2 plasma-treated passive films on ground MgZn2 (a), Mg (b), and Zn (c) substrates, with spectra obtained from the surfaces after the respective cleaning step in an Ar/H2 plasma as references. From Giza et al.[30]

3.2. Plasma-Semiconductor Interfaces

The interaction of plasmas with semiconductors is of paramount importance for applications in microelectronics. During processing of integrated circuits, several 100 process steps are necessary, involving the deposition and etching of thin layers. The majority of those steps are based on plasma processes where silicon or silicon oxide is being etched by halogen containing plasmas. By choosing, for example, the proper fluorocarbon source gas and the ion bombarding energy of the plasma, selective and anisotropic etching processes are realized. The erosion mechanisms are governed by a fluorocarbon top layer that is present during steady state etching, which allows for chemical sputtering of the silicon material.[33] The composition and thickness of those fluorocarbon top layers are often monitored by infrared spectroscopy.[34]

A further prominent example is the deposition of amorphous hydrogenated silicon films as being used for thin film solar cells. The analysis of the plasma chemistry indicates that SiH_3 is the dominant radical for the deposition of high quality a-Si:H films.[35] Consequently, the surface reaction of SiH_3 on an a-Si:H surface had been in the focus of the research interest and had also been investigated by

DOI: 10.1002/ppap.201500087

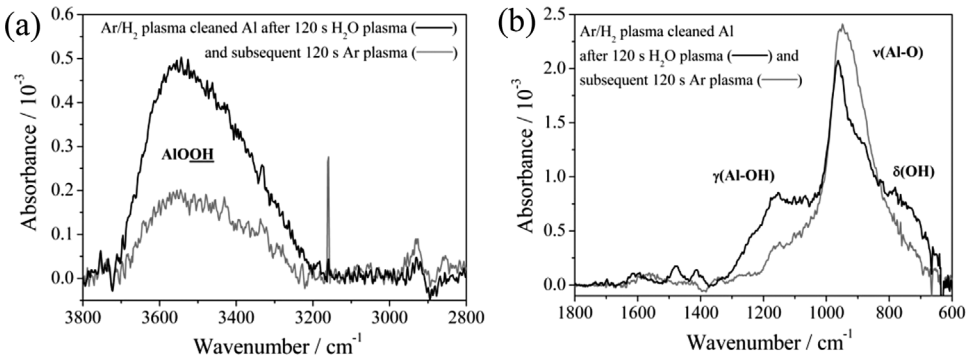

Figure 9. In situ FT-IRRAS spectra of an oxide-covered Al surface after a water and subsequently argon plasma modification related to the background acquired after the cleaning step: (a) region of OH vibrations (3800–2800 cm^{-1}), (b) region of Al–O, Al–OH, and H_2O vibrations (1800–600 cm^{-1}). From Giza et al.[31]

infrared spectroscopy. The understanding of the surface reaction of SiH_3 on an a-Si:H surface is challenging, because the reaction probability for an SiH_3 radical is typically at 10% although the a-Si:H surface is almost 100% H terminated during thin film growth. If one assumes a sequential growth mechanism, where a surface hydrogen has to be abstracted to create a dangling bond before an SiH_3 radical can chemisorb at this site, a hydrogen surface coverage of only 90% would be expected. This puzzle has been addressed by postulating a "hot precursor" mechanism, where an incident SiH_3 does not thermalize at the surface upon impact but rather diffuses at the surface and samples many surface sites before chemisorption takes place.

This postulated reaction scheme has been tested by HD exchange experiments starting with a deuterated a-Si:D film.[36] This film is exposed to a plasma based SiH_3 source. Figure 10 shows the resulting changes in the reflectivity spectra. The decrease in reflectivity at ~2090 cm^{-1} after 98 s indicates the creation of SiH surface groups consisting predominantly of monohydrides; the decrease in reflectivity at ~2000 cm^{-1} at 392 s indicates the creation of SiH bulk modes and corresponds to the onset of bulk film growth. The increase in reflectivity at 1515 cm^{-1} indicating the removal of SiD surface groups becomes visible only after 392 s, and saturates after 780 s. The reflectivity at 1455 cm^{-1} increases slightly during longer exposure times, indicating a slow release of SiD bulk groups. These spectra show that SiH groups are created before the removal of SiD groups, which contradicts the postulated sequence of creation of a dangling bond by deuterium abstraction followed by SiH_3 chemisorption. According to this sequence, the change in SiH groups should occur simultaneously with the change in SiD groups. This is not observed. This puzzle has been resolved by postulating a SiH_3 insertion mechanism at strained Si-Si bonds at the film surface. It is known that atomic hydrogen can easily insert into strained dimers at the 2×1 reconstructed Si(100) surface to form the 1×1 reconstruction. The incoming SiH_3 radical follows an analogous reaction pathway. The insertion of a SiH_3 radical into strained Si-Si bonds on the growing a-Si:H film surface will form at first a transition state consisting of a penta-coordinated SiH_3 site:

$$SiH_{3(g)} + Si{-}Si_{(s)} \rightarrow Si{-}SiH_3{-}Si_{(s)}$$

the indices (s) and (g) denote the surface and gas phase, respectively. The existence of penta-coordinated silicon

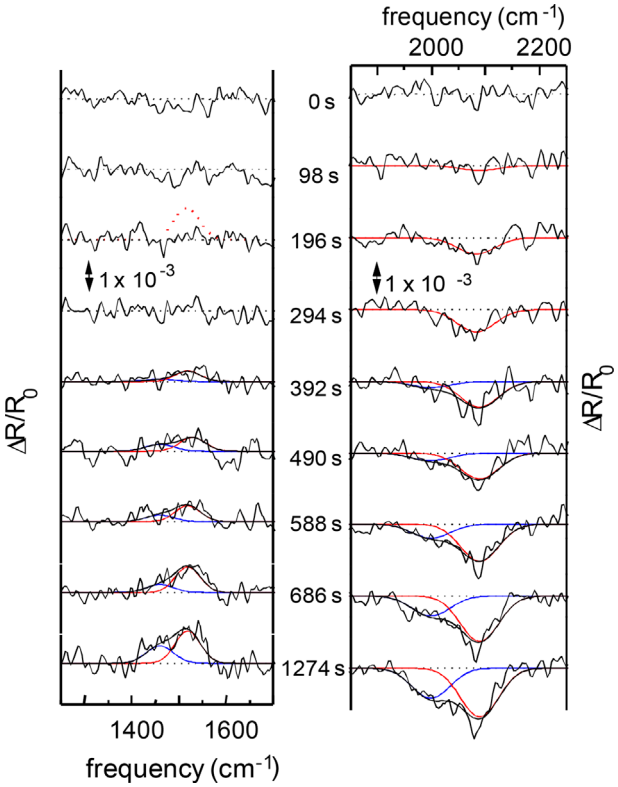

Figure 10. OCS FTIR data for SiH stretching vibrations (right side) and SiD stretching vibrations (left side). The figure shows the change in the reflectivity during exposure of the a-Si:D film. From ref.[36]

atoms is well known as a transition state in nucleophilic substitution reactions. The penta-coordinated silicon atoms are bonded through their dsp^3 orbitals as known for fivefold coordinated Si compounds in the gas phase. In the case of adsorption of SiH_3 at the hydrogenated surface, this situation is reversed, as now the dangling bond of the SiH_3 radical acts as the donor and the silicon atom on the surface acts as the acceptor for the charge transfer during bonding. This insertion mechanism does not require a preceding H abstraction mechanism. This postulated insertion of SiH_3 in the strained bonds at an a-Si:H surface has been later supported by molecular dynamics modeling calculations.[37]

3.3. Plasma-Polymer Interfaces

The performance of polymers is often dominated by interface properties such as wettability, friction, lubrication, adhesion, and compatibility with applied coatings.[38] ATR-FTIR spectroscopy is often the preferred analytical technique in such cases especially when surfaces of bulk polymer materials are studied.

Plasma modification on polyethylene[39] and polystyrene[40] was evaluated ex situ by ATR-FTIR. Geyter et al.[39] investigated the plasma modifications induced by a dielectric barrier discharge in air at medium pressure on polyethylene. The polymer modifications were investigated by contact angle measurements and ex situ ATR-FTIR. It was found that plasma treatment introduced oxygen-containing functionalities, such as ketones, aldehydes, alcohols, and carboxylic acids on the PE surface leading to the increased surface free energy. ATR-FTIR spectroscopy was used to detect these oxygen-containing groups. Additionally, polyethylene and polystyrene modifications due to plasma exposure were also investigated by Guruvenket et al.[40] The plasmas in this case were Ar and O_2 glow plasmas in a low pressure microwave discharge. ATR analysis of oxygen-treated polymer surface showed several oxygen-based functionalities at the surface (carbonyl, carboxyl, ether, peroxide, etc.). The contact angle measurements done on the oxygen plasma-treated polystyrene and polyethylene samples indicate the fast transformation to the hydrophilic nature compared to the polyethylene and polystyrene samples treated with the argon plasmas. It can also be observed that the treatment time/power required to bring down the contact angle using oxygen plasma is much less than the treatment time/power required to bring down the contact angle using argon plasma.

Apart from strictly FTIR-dedicated research, the technique of ex situ ATR-FTIR is widely employed in combination with several other surface characterization methods,[41] or for the characterization of particularly challenging substrates, such as for example plasma-modified wood surfaces.[42] It can also be applied in order to obtain quantitative information, as shown by Klage and Grishin[43] who developed a method to quantify the density of functional groups from ATR measurements. The method allows to determine the area densities ρ (numbers or mole numbers per unit area) of chemical functional groups. As an example, they applied the method to polymer surfaces plasma aminated in atmospheric pressure afterglows of $N_2 + H_2$ mixtures. The procedure is based on the assumption of equal molar absorption coefficients for the characteristic vibrations in the surface polymer and a reference solution.

The real strength of the ATR technique, however, is made manifest when applied in situ for the investigation of either plasma modification of polymers,[44] or plasma polymerization.[45] In the work of Nitschke and Meichsner[44] two model polymers, polyethylene, and polystyrene, were treated in radio-frequency (rf) discharges in argon, hydrogen, oxygen, nitrogen, and tetrafluoromethane. The in situ IR characterization methods employed were IRRAS and ATR. Figure 11 shows the ATR spectra of polyethylene during different plasma treatments. The negative bands at 2950–2700 cm^{-1}

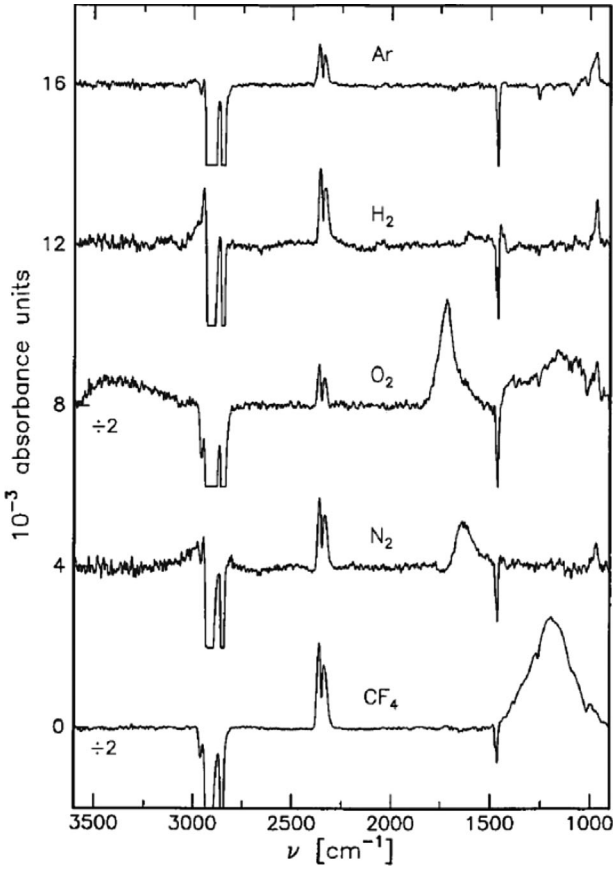

Figure 11. Figure from Nitschke et al.,[44] showing the in situ ATR spectra of polyethylene during different plasma treatments.

DOI: 10.1002/ppap.201500087

and 1460 cm^{-1} (CH_2 stretching and bending) visible in the spectra of argon- and hydrogen-plasma treated polymer indicate modifications related to hydrogen abstraction; the positive bands at 980–965, 3000–2950, and 1450–1410 cm^{-1} indicate possible cross-linking. Exposure to oxygen or nitrogen plasmas reveals a second group of effects involving the formation of structures containing foreign atoms. In the case of oxygen plasma, this relates to the formation O—H groups (at 3600–3000 cm^{-1}), or carbonyl (1800–1960 cm^{-1}). Exposure to nitrogen plasma on the other hand results mostly in the appearance of a positive band at 1725–1500 cm^{-1}, attributed to C═N groups.

Klages et al.[46] performed in situ ATR for the investigation of the surface modification of Polyolefins by atmospheric pressure dielectric barrier discharges in nitrogen containing gases. The goal in this case was to understand the plasma-induced generation of chemical functional groups on polymer surfaces and their temporal development in the presence of inert or reactive atmospheres. The temporal dependence was established by measuring FTIR spectra at intervals of 10 s, during and after plasma treatment of the substrate. They showed that the reaction of nitrogen-plasma-treated polymer surfaces with TFBA (4-trifluoromethyl-benzaldehyde) was not selective for primary amino groups.

Additional in situ monitoring by IRRAS and ATR of plasma surface modification of polymers (polystyrene and polyethylene) and their plasma polymerization is found in the work of Meichsner.[45] In particular case of plasma polymerization, a novel fiber-ATR technique was applied to investigate the plasma polymerization process in the plasma bulk. Figure 12 shows the FTIR-spectrum of a thin plasma polymerized styrene film on the fiber in comparison to dip coated polystyrene and plasma polymerized styrene

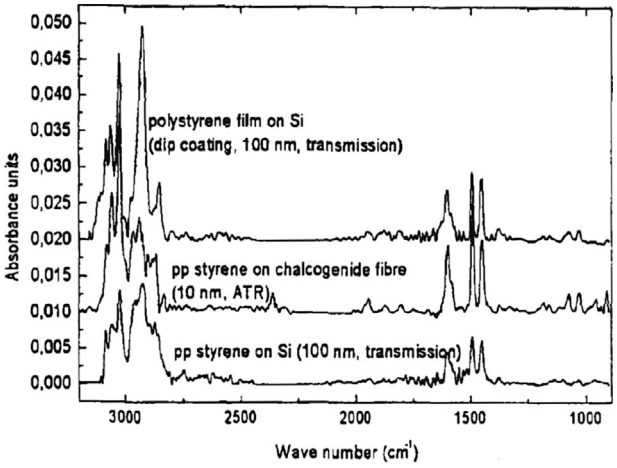

Figure 12. Figure from Meichsner,[45] showing the FTIR-spectrum of plasma polymerised styrene film using fibre-ATR compared with spectra of plasma polymerized styrene and polystyrene obtained by transmission technique.

on plane silicon wafer using FTIR-transmission technique. The relatively sharp peaks of the aromatic ring structures and the symmetric and asymmetric CH– stretching vibrations at 2900 cm^{-1} can be seen clearly. The sensitivity is much higher using the ATR-technique (lower film thickness in respect to the transmission experiment). In contrast to the polystyrene film, the plasma polymerized styrene shows a broader band in the aliphatic C—H-structure. The plasma polymer is characterized by an amorphous and cross linked structure with no uniform molecular surroundings.

In order to investigate plasma modification on polymer surfaces, very high sensitivity is required, because ions and neutrals affect the surface only within a penetration depth of the order of a few nanometers at most. The enhancement of sensitivity can be achieved by using the previously described OCS,[47–49] or by depositing ultra-thin polymer films on smooth gold substrates to allow for the application of PM-IRRAS.[50]

In Große-Kreul et al. and Corbella et al.,[47–49] the etching and chemical modification of different polymers was monitored in real-time by in situ IRRAS using OCS substrates, with a thickness of the oxide layer to 1 μm in order to achieve the condition of resonance with the infrared wavelength of the probing light (Figure 4). With this arrangement they could resolve reflectivity changes of the order of $\Delta R/R_0 \cong 10^{-4}$ corresponding to the removal of sub-monolayers of polymer (where R_0 corresponds to the spectrum of the pristine polymer). The polymer modification was done in these cases within a particle beam experiment where quantified beams of Ar ions and/or reactive species such as oxygen can be manipulated separately. Such setups (Figure 13) aim to determine the polymer modification due to different species separately, and to investigate possible synergies. This setup was applied for the investigation of PET and PP modified with Ar ions and O atoms using both in situ IRRAS and QCM.[47–49] Thanks to this setup, the interactions of VUV photons and ions on polymer surfaces (etching and cross-linking) were analyzed, as well as the role played by reactive species in the chemical sputtering of PET and PP. Moreover, time-resolved FTIR measurements of layer absorbance permitted to model the modified top layer of polymers during plasma treatment.

Ozkaya et al.[50] employed PM-IRRAS to investigate interfacial processes during the initial stages of SiO_x-like plasma-polymer barrier coating deposition, using as substrates octadecanethiol (ODT) self-assembled monolayers on Au-film coated wafers. The precise positions of the ODT peaks in the FTIR spectra (Figure 14) allowed to estimate the degree of order and crystallinity of the prepared monolayer before and after plasma-deposition of films. Their results indicated that oxygen-rich deposition of a SiO_x barrier layer lead to an oxidative degradation of the

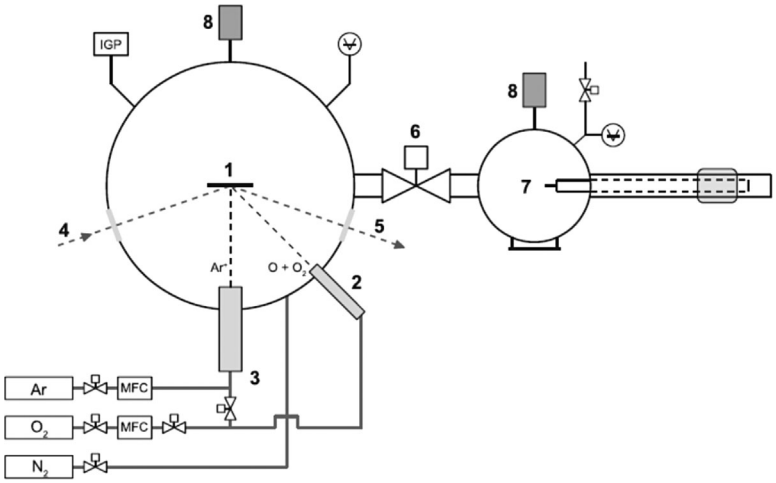

Figure 13. Schematic of a particle beam experiment for the in-situ characterization of polymer modification by ATR from Große-Kreul et al.[47] (1), oxygen capillary source (2), plasma ion source (3). The infrared beam passes the chamber via windows (4) and (5) and impinges onto the sample at an angle of incidence of 70°. (6) Valve; (7) load lock; (8) turbomolecular pump; (9) transfer rod.

polymer-like substrate layer. This indicates that adhesive failure or delamination of plasma-deposited barrier layers on polymeric substrates can be caused by deposition of the SiO_x barrier film when employing an oxygen-rich plasma.

3.4. Special Applications of SEIRA and SFG

The first application of SEIRA to the investigation of plasma modification of surfaces was done in 1999, by Geng et al.[51] Using a CaF_2 substrate covered with thin layers of Au or Ag, SEIRA was used to investigate the surface modification of molecular layers of stearic acid (to simulate the reactions of a polyethylene surface with plasma) by O_2 and NH_3 plasma, and the plasma polymerization of alylamine. Hanus et al.[52] investigated the interface between a polymer-like C:H matrix and Ag particles on Ag/C:H composite films deposited by magnetron sputtering, which also worked as SEIRA active substrates. They could show the existence of a very thin interface region between plasma polymer C:H and Ag nanocluster surface due to an oxidized plasma polymer with carbonyl, carboxylate, and carbonate species bound directly to the silver.

The idea of using surfaces with inherent enhancing capabilities such as silver, in combination with in situ IRRAS for the investigation of metal-polymer interfaces is further developed by Hlídek et al.[53] who performed an exhaustive analysis of the evolution of silver interfaces in nanocomposite materials consisting of polymeric matric with silver inclusions deposited by magnetron sputtering.

Chen et al.[38] reviews in situ detection at the molecular level of surface structures of some common polymers in air (PE, PP, PS, PMMA, polyimides, PEG, and polyurethanes). Applying the SFG technique, surface changes such as surface segregation of small end groups, polymer surface restructuring in water, and stepwise changed polymer blend surfaces could be investigated. Studies of surface glass transition and surface structures modified by rubbing, plasma deposition, UV light irradiation, oxygen ion and radical irradiation, and wet etching are also discussed.

Apart from exposure to charged species or reactive species, recombination processes in plasmas lead to the emission of UV radiation, which by itself can also induce dramatic changes on polymer surfaces. The separate effects of UV irradiation and plasma treatment were studied by IR-visible sum frequency generation spectroscopy (SFG) by ref.[54] on polystyrene, and by ref.[55] on poly (dimethylsiloxane).

Zhang et al.[54] observe spectral changes, similar for UV irradiation and plasma treatment, that indicate the occurrence of surface reactions involving the aromatic structures, leading to loss of aromaticity. They also observed oxidation in both cases, but in degrees different for both processes. In particular, the oxidation to a higher oxidation state, resulting in the formation of carbonyl/carboxyl species, was observed with plasma treatment but not with UV irradiation alone. They propose that the uptake of oxygen by the phenyl group, resulting in a phenol-like species, is the main pathway for UV irradiation, while an oxidative attack of the benzene ring, followed by a ring opening to form aldehyde/carboxylate species, is the main mechanism for plasma treatment.

Ye et al.[55] investigated the kinetics of poly (dimethylsiloxane) (PMDS) surface modification. They differentiated the effect of exposure to long- and short-wavelength UV, and exposure to oxygen RF-plasma. SFG was performed in air and in situ during the UV-exposure experiments, while the measurements of plasma modification were done in air immediately after plasma exposure (18 W rf plasma source). They observed that CH_3 and CH_2 groups on the surface decreased during all three modification processes and Si–OH groups were detected. The change of CH_3 groups at the surface followed first-order kinetics and was seen to be fastest for plasma, followed by short λ UV (UV) exposure. Long λ UV (UVO) exposure had the least effect of the polymer surface. Compared to UV, UVO irradiation at 185 and 254 nm in air is associated with generation of atomic oxygen, a strong oxidizing agent. An oxygen plasma, on the other hand, consists of a large number of electrons and highly reactive ionic and free radical oxygen species that

DOI: 10.1002/ppap.201500087

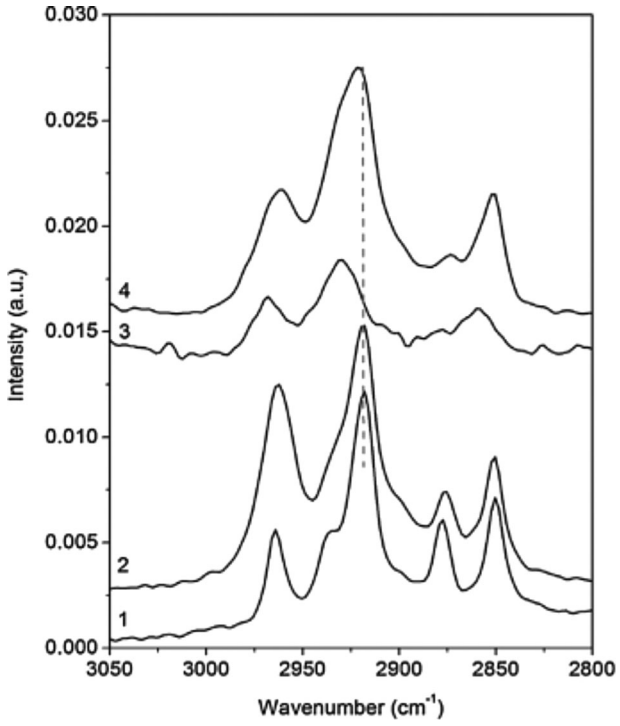

Figure 14. PM-IRRAS data of SiO_x-like barrier films and adhesion promoting interlayers deposited on ODT covered Au substrates. 1) ODT reference, 2) deposition of SiOCH from an oxygen-free plasma, 3) deposition of SiO_x from an oxygen-containing plasma, and 4) deposition of SiO_x onto a SiOCH adhesion-promoting layer. The band at 2965 cm^{-1} is assigned to CH_3 assymetric in-plane CH stretching mode; bands at 2879 and 2937 cm^{-1} are symmetric CH stretching vibrations of CH_3 groups. The band at 2850 cm^{-1} belongs to symmetric CH_2 stretching, and that at 2917 cm^{-1} is assigned to the CH_2 asymmetric stretching vibration. Shifts towards higher wavenumbers of the band marked with the dotted line indicate a disordered layer; shifts towards lower wavenumbers indicate that the alkyl chains adopt an all-trans conformation. Figure from Ozkaya et al. [50]

facilitate oxidation of surfaces. At steady state, plasma modification transformed the PDMS surface from a CH_3-terminated surface to one almost devoid of CH_3 groups, whereas UV modification leaves different fractions of CH_3 groups on the surface depending on the specific wavelength used, which suggests that it should be possible to tailor the fraction of hydroxyl groups at the surface precisely using the appropriate modification technique.

4. Conclusions and Outlook

Infrared reflection spectroscopy is a very powerful tool for the in situ and ex situ characterization of surfaces and interfaces in plasma surface technology. Its main strength lays in the capability to perform in situ analysis of chemical groups ranging from monolayers to thin films over a wide pressure range with high sensitivity.

The future challenge will be to increase even further the surface sensitivity over a wide wavenumber range and to increase the temporal resolution in order to, for example, unravel the changes in surface composition in pulsed plasmas in the kHz range. If those processes would be strictly periodical, the well known step-scan method could be used by a synchronized integration of the signal over many pulses to reach a sufficient sensitivity. However, in most cases, either a film is being continually etched or is continually growing, which makes the step scan method inapplicable, since the surface conditions change from pulse to pulse. Therefore, the goal is to achieve high sensitivity in single shot measurements. Most infrared light sources, though, exhibit rather low intensities. As a consequence, future infrared surface diagnostics employing tuneable infrared lasers should be developed to improve sensitivity and temporal resolution. If those lasers are pulsed, elaborate schemes such a cavity ring down could be employed to reach ultimate sensitivities in the IR range.

Acknowledgements: The DFG (German Research Foundation) within the framework of the Special Research Field SFB-TR 87 is acknowledged. Fruitful discussions with Drs. I. Giner, A. Keller, and C. Corbella are also gratefully acknowledged.

Received: May 28, 2015; Revised: June 29, 2015; Accepted: June 30, 2015; DOI: 10.1002/ppap.201500087

[1] W. Suëtaka, *Methods of Surface Characterization*, Vol. *3*, Plenum Press, New York **1995**.
[2] Y. J. Chabal, *Surf. Sci. Rep.* **1988**, *8*, 211–357.
[3] N. J. Harrick, *Internal reflection spectroscopy*, 3rd edition, Interscience, New York **1967**.
[4] J. McIntyre, D. E. Aspnes, *Surf. Sci.* **1971**, *24*, 417.
[5] J. Umemura, T. Kamata, T. Kawai, T. Takenaka, *J. Phys. Chem.* **1990**, *94*, 62.
[6] T. Buffeteau, B. Desbat, J. M. Turlet, *Appl. Spectrosc.* **1991**, *45*, 380.
[7] G. Grundmeier, E. Matheisen, M. Stratmann, *J. Adhesion Sci. Technol.* **1996**, *10*, 573.
[8] M. Maxisch, In-Situ-FTIR- Spectroscopic Studies of Organic Acid Monolayers on Metal Oxides in Humid Environments, *Dissertation. University of Paderborn, Germany* **2011**.
[9] M. Katiyar, *J. Vac. Sci. Technol. A* **1995**, *13*.
[10] 10a M. Katiyar, Y. H. Yang, J. R. Abelson, *J. Appl. Phys.* **1995**, *77*, 6247. 10b M. Katiyar, Y. H. Yang, J. R. Abelson, *J. Appl. Phys.* **1995**, *78*, 1659.
[11] A Von Keudell, JR Abelson, *J. Appl. Phys. 91* **2002**; 4840
[12] M. Born, E. Wolf, *Principles of Optics: Electromagnetic Theory of Propagation, Interference and Diffraction of Light*, 7th edition, Cambridge University Press, Cambridge, New York **1999**.
[13] P. Grosse, B. Harbecke, B. Heinz, R. Meyer, M. Offenberg, *Appl. Phys. A* **1986**, *39*, 257.
[14] H. R. Philipp, *J. Appl. Phys.* **1979**, *50*, 1053.

[15] B. Harbecke, B. Heinz, P. Grosse, *Appl. Phys. A* **1985**, *38*, 263.
[16] B. Harbecke, *Appl. Phys. B* **1986**, *39*, 165.
[17] A. E. Bjerke, P. R. Griffiths, W. Theiss, *Anal. Chem.* **1999**, *71*.
[18] R. Aroca, B. Price, *J. Phys. Chem. B* **1997**, *101*, 6537.
[19] O. Krauth, G. Fahsold, A. Pucci, *J. Chem. Phys.* **1999**, *110*, 3113.
[20] M. Osawa, M. Ikeda, *J. Phys. Chem.* **1991**, *95*, 9914.
[21] S. Kawata, *Topics in Applied Physics*, Springer, New York **2001**, vol. *81*.
[22] D. Ross, R. Aroca, *J. Chem. Phys.* **2002**, *117*, 8095.
[23] M. S. Anderson, *Appl. Phys. Lett.* **2003**, *83*, 2964.
[24] T. R. Jensen, Duyne, R. P. Van, S. A. Johnson, V. A. Maroni, *Appl. Spectrosc.* **2000**, *54*, 371.
[25] S. Cataldo, J. Zhao, F. Neubrech, B. Frank, C. Zhang, P. V. Braun, H. Giessen, *ACS nano* **2012**, *6*, 979.
[26] C. D'Andrea, J. Bochterle, A. Toma, C. Huck, F. Neubrech, E. Messina, B. Fazio, O. M. Maragò, E. Di Fabrizio, M. Lamy de La Chapelle, P. G. Gucciardi, A. Pucci, *ACS Nano* **2013**, *7*, 3522.
[27] J. M. Hoffmann, X. Yin, J. Richter, A. Hartung, W. W. Tobias Maß, T. Taubner, *J. Phys. Chem. C* **2013**, *117*, 11311.
[28] S. Bagheri, H. Giessen, F. Neubrech, *Adv. Optical Mater.* **2014**, *2*, 1050.
[29] J. Raacke, M. Giza, G. Grundmeier, *Surf. Coat. Technol.* **2005**, *200*, 280–283.
[30] M. Giza, G. Grundmeier, *Plasma Process. Polym.* **2011**, *8*, 607–616.
[31] M. Giza, P. Thissen, G. Grundmeier, *Langmuir* **2008**, *24*, 8688.
[32] I. Giner, M. Maxisch, C. Kunze, G. Grundmeier, *Appl. Surf. Sci.* **2013**, *283*, 145–153.
[33] H. F. Winters, J. W. Coburn, *Surf. Sci. Rep.* **1992**, *14*, 162.
[34] B. Zhou, E. A. Joseph, L. J. Overzet, M. J. Goeckner, *J. Vac. Sci. Technol. A* **2006**, *24*, 114.
[35] W. M. M. Kessels, K. Nadir, M. C. M. van de Sanden, *J. Appl. Phys.* **2006**, *99*, 076110.
[36] A. von Keudell, J. R. Abelson, *Phys. Rev. B* **1999**, *59*, 5791.
[37] S. Agarwal, M. S. Valipa, B. Hoex, M. C. M. van de Sanden, D. Maroudas, E. S. Aydil, *Surf. Sci.* **2005**, *598*, 35.
[38] Z. Chen, Y. R. Shen, G. A. Somorjai, *Annu. Rev. Phys. Chem.* **2002**, *53*, 437.
[39] N. de Geyter, R. Morent, C. Leys, *Surf. Interface Anal.* **2008**, *40*, 608.
[40] S. Guruvenket, G. M. Rao, M. Komath, A. M. Raichur, *Appl. Surf. Sci.* **2004**, *236*, 278.
[41] (a) F. Lewis, S. Turgeon, P. Chevallier, J.-J. Pireaux, M. Tatoulian, D. Mantovani, *Plasma Process. Polym.* **2010**, *7*, 309. (b) A. Kondyurin, O. Polonskyi, N. Nosworthy, J. Matousek, P. Hlidek, H. Biederman, Bilek, M. M. Marcela, *Plasma Process. Polym.* **2008**, *5*, 727.
[42] O. Levasseur, L. Stafford, N. Gherardi, N. Naudé, V. Blanchard, P. Blanchet, B. Riedl, A. Sarkissian, *Plasma Process. Polym.* **2012**, *9*, 1168.
[43] C.-P. Klages, A. Grishin, *Plasma Process. Polym.* **2008**, *5*, 359.
[44] M. Nitschke, J. Meichsner, *J. Appl. Pol. Sci* **1997**, *65*, 381.
[45] J. Meichsner, *Contrib. Plasma. Phys.* **1999**, *39*, 427.
[46] C.-P. Klages, A. Hinze, Z. Khosravi, *Plasma Process. Polym.* **2013**, *10*, 948.
[47] S. Große-Kreul, C. Corbella, A. von Keudell, *Plasma Process. Polym.* **2013**, *10*, 225.
[48] S. Große-Kreul, C. Corbella, A. von Keudell, B. Ozkaya, G. Grundmeier, *Plasma Process. Polym.* **2013**, *10*, 1110.
[49] C. Corbella, S. Große-Kreul, A. von Keudell, *Plasma Process. Polym.* **2015**, *12*, 564.
[50] B. Ozkaya, F. Mitschker, O. Ozcan, P. Awakowicz, G. Grundmeier, *Plasma Process. Polym.* **2015**, *12*, 398.
[51] S. Geng, J. Friedrich, J. Gähde, L. Guo, *J. Appl. Pol. Sci* **1999**, *71*, 1231.
[52] J. Hanus, M. Drabik, P. Hlidek, H. Biederman, G. Radnoczi, D. Slavinska, *Vacuum* **2008**, *83*, 454.
[53] (a) P. Hlídek, H. Biederman, A. Choukourov, D. Slavínská, *Plasma Process. Polym.* **2008**, *5*, 807. (b) P. Hlídek, H. Biederman, A. Choukourov, D. Slavínská, *Plasma Process. Polym.* **2009**, *6*, 34.
[54] D. Zhang, S. M. Dougal, M. S. Yeganeh, *Langmuir* **2000**, *16*, 4528.
[55] H. Ye, Z. Gu, D. H. Gracias, *Langmuir* **2006**, *22*, 1863.
[56] http://commons.m.wikimedia.org/wiki/File:Principe_PM-IRRAS.png, figure licensed under the Creative Commons Attribution-Share Alike 4.0 International license.

DOI: 10.1002/ppap.201500087